Submitted to the
International Europhysics Conference on High Energy Physics
July 17 - 23, 2003, Aachen, Germany

Abstract: 544 **Session: HQCD, HP**

Study of DIS events containing a leading proton in e^+p collisions at HERA

ZEUS Collaboration

Abstract

The semi-inclusive differential cross sections $d\sigma_{ep\to eXp}/dx_L$, $d\sigma_{ep\to eXp}/dp_T^2$ and $d^2\sigma_{ep\to eXp}/dx_L dp_T^2$ are measured in deep-inelastic e^+p collisions at HERA at $\sqrt{s} = 300$ GeV and for virtualities of the exchanged photon $Q^2 > 3$ GeV^2. The measurement is performed in the kinematic range of the final-state proton $x_L > 0.56$ and $p_T^2 < 0.5$ GeV^2, where x_L is the fraction of the proton-beam longitudinal momentum carried by the final-state proton and p_T^2 its transverse-momentum squared. The data sample of $12.8\,\mathrm{pb}^{-1}$ used for this study was collected with the ZEUS detector during the 1996-97 data taking period. The leading protons were measured in the ZEUS leading-proton spectrometer.

1 Introduction

Leading-proton production below the diffractive peak has been studied in proton-proton collisions, both at the ISR [1, 2] and in fixed-target experiments [3, 4]. More recently, the HERA-collider experiments measured the production of leading-protons in ep collisions [5–7]. With these few exceptions, the experimental data are scarce. This lack of information is a problem for a deep understanding of strong interactions beyond the perturbative expansion of QCD. Indeed, in high-energy collisions, the QCD-hardness scale decreases from the central, large p_T region, to the the soft, non-perturbative hadronic scale of the target-fragmentation region. Therefore, the detection of leading protons in the final state of high-energy collisions yields information on the non-perturbative side of strong interactions. Another reason for the interest in leading-proton production comes from the fact that the ISR data revealed universality features of the hadronic final states produced in electro-weak and strong interactions if the hadronic systems are analysed in terms of the effective energy available for hadronization [8]. In deep-inelastic scattering (DIS), the effective energy can be obtained with a good approximation using the four-momenta of the scattered lepton and of the leading proton detected in the final state. For these reasons, a large-statistics sample of DIS events containing a leading proton measured with high precision is highly desirable.

In this paper, we present a measurement of the cross-section for the semi-inclusive reaction $ep \to eXp$ in deep-inelastic scattering at HERA. The final state protons, scattered at high energies and small transverse momenta, were detected in the leading-proton spectrometer [9] of the ZEUS detector. The single-differential cross sections $d\sigma_{ep\to eXp}/dx_L$ and $d\sigma_{ep\to eXp}/p_T^2$, and the double-differential cross section $d^2\sigma_{ep\to eXp}/dx_L dp_T^2$ were measured in the kinematic range $Q^2 > 3\,\mathrm{GeV}^2$ and $45 < W < 225$ GeV, where W is the total mass of the hadronic system. The protons were measured in the range $x_L > 0.56$ and $p_T^2 < 0.5$ GeV^2, where x_L represents the fractional longitudinal momentum of the proton and p_T its transverse momentum. The $12.8\,\mathrm{pb}^{-1}$ data sample used for this study was collected during the 1996 and 1997 data-taking periods.

2 The ZEUS detector

The components of the ZEUS detector [10] most relevant for this study are the calorimeter (CAL) the central tracking detector (CTD) and the leading proton spectrometer (LPS).

The CAL [11] is a Uranium-scintillator calorimeter which provides a polar-angle[1] coverage $2.6^\circ < \theta < 176.2^\circ$; relative energy resolutions of $\sigma(E)/E = 0.18\sqrt{E}$ (E in GeV) for electromagnetic showers and $\sigma(E)/E = 0.35\sqrt{E}$ for hadronic showers have been measured in a test beam.

The CTD [12] is a cylindrical drift chamber which operates in a magnetic field of 1.43 T provided by a thin superconducting coil and covers the polar-angle region $15^\circ < \theta < 164^\circ$. The relative transverse-momentum resolution for full-length tracks is $\sigma(p_t)/p_t = 0.0058p_t \oplus 0.0065 \oplus 0.0014/p_t$, with p_t in GeV.

The LPS [9] was utilised during the 1994-2000 data taking period to detect positively charged particles scattered at very small angles and carrying a large fraction of the incoming-proton beam momentum. It was made by 36 planes of silicon microstrip detectors grouped in six stations, S1 to S6, and placed along the beam line in the direction of the proton beam, between Z = 20 m and Z = 90 m. During data taking, the stations were inserted very close to the proton beam (typically few mm). Charged particles inside the beampipe were deflected by the magnetic field of the proton-beamline magnets and measured in the LPS with resolutions better than 1% on the longitudinal momentum and of 5 MeV on the transverse momentum. The proton-beam emittance of ≈ 40 MeV in the horizontal plane and ≈ 90 MeV in the vertical plane dominated the transverse-momentum resolution. For this study, only stations S4, S5 and S6 were used.

3 The data sample and the event selection

During the 1996-97 data taking period, the ZEUS detector collected $12.8\,\mathrm{pb}^{-1}$ in which the experimental conditions allowed the LPS to be inserted close to the proton beam and be operational. A three-level trigger was used to select the data online, each level being more selective than the previous one. At the third level, the event variables were reconstructed in the CAL and CTD with an accuracy close to that obtained off-line; the presence of a reconstructed track in the LPS was also required.

Final detector calibration and full-event reconstruction were performed off-line. The following requirements were imposed:

- $|V_Z| < 50$ cm, where V_Z is the Z coordinate of the reconstructed vertex;
- a scattered positron with energy $E'_e > 10$ GeV reconstructed in the CAL outside the region close to the rear beam-pipe hole where the presence of inactive material reduced

[1] The ZEUS coordinate system is a right-handed Cartesian system, with the Z axis pointing in the proton beam direction, referred to as the "forward direction", and the horizontal X axis pointing left towards the centre of HERA. The coordinate origin is at the nominal interaction point.

the precision of the energy measurement;

- the $E - p_Z$ of all the energy deposits in the CAL, excluding those assigned to the scattered positron, in the range $38 < E - p_Z < 65$ GeV;
- exchanged-γ virtuality $Q^2 > 3$ GeV^2 and total hadronic mass $45 < W < 225$ GeV;
- the hadronic variable y_{JB} [13] was required to exceed 0.03 in order to ensure hadronic activity away from the forward direction;
- a reconstructed track in the LPS having $p_T^2 > 0.5$ GeV^2 and $x_L > 0.56$. To reduce the sensitivity of the LPS acceptance to the uncertainty on the location of the beam-pipe apertures, the minimum track distance from the beampipe was required to be $\Delta_{pipe} > 0.04$ cm. The selection of tracks with $\Delta_{pot} > 0.02$ cm, where Δ_{pot} is the minimum distance of the track from the edge of any LPS detector, ensured that the tracks were well within the active region of the silicon detectors;
- the sum of the energy deposits in the CAL and of the LPS track, $E + P_Z$, was required to be smaller than 1655 GeV; this cut rejected most of the random overlays of a DIS event in ZEUS and a leading proton from beam-halo or proton-gas collision in the LPS.

A total of 71,937 events survived the above selection criteria.

4 The Montecarlo samples

To determine the acceptance of the apparatus, ten million DIS events with $Q^2 > 2$ GeV^2 were generated using Djangoh [14]. This sample was also used to study the migration of events from low Q^2, together with a sample of 500,000 Djangoh events with $0.5 < Q^2 < 2$ GeV^2 and one million photoproduction events generated with Pythia [15]. The two Djangoh samples include diffractive events, produced by this generator using the soft-colour-interaction mechanism.

All Montecarlo (MC) events were passed through the standard simulation of the ZEUS trigger and detector, and through the same reconstruction and analysis programs as the data. The simulation included the geometry of the beam-pipe apertures, the magnetic field along the leading proton trajectory and the proton-beam emittance.

To have a good description of the data, it was necessary to reweight the leading-proton x_L and p_T^2 distributions generated by the MC; the fraction of diffractive events w.r.t. the total was also reweighted in bins of x_L. In particular, the slope of the exponential p_T^2 distribution was reweighted from the generated average value $\langle\, b \,\rangle \approx 3.6$ GeV^{-2} to $b = 7$ GeV^{-2}.

Figure 1 shows the distribution of several CAL and LPS quantities as measured in the data and compared to the sum of the reweighted MC samples. The agreement is generally good. The reweighting produced a better agreement not only in the x_L and p_T^2 distributions, but also in the W and in the other distributions related to the leading proton.

The Djangoh sample was also used to subtract the fraction of tracks reconstructed in the LPS which are due to π^+ and K^+, as described in section 6.

5 Acceptance

To ensure a high purity in each of the x_L, p_T^2 bins of the analysis, bins of 0.03 units of x_L and between 0.05 GeV^2 and 0.150 GeV^2 in p_T^2 were used; these bin widths correspond to at least twice the LPS resolution as obtained from the MC. The acceptance was defined as the ratio of the number of reconstructed events in a x_L, p_T^2 bin to the number of generated events in that bin. This definition includes the effects of the geometrical acceptance of the apparatus, its efficiency and resolution, and the event selection efficiency. Figure 2 shows the acceptance of LPS stations S4, S5 and S6. The bins in the x_L, p_T^2 plane in which the acceptance was either rapidly varying or below 1% were excluded from the analysis. These requirements restricted the measurement to $p_T^2 \lesssim 0.3$ GeV^2 in the $0.7 \lesssim x_L \lesssim 0.8$ and $x_L > 0.95$ ranges, and to $p_T^2 < 0.5$ GeV^2 elsewhere. The region $x_L < 0.56$ was also excluded due to the limited acceptance in p_T^2 in this range of x_L.

6 Backgrounds and migrations

Three sources of possible background contamination of the data were considered:

- positive pions and kaons produced at very small angles are reconstructed by the LPS if they pass through the active area of the detector. This background was estimated using the MC and subtracted in each bin of the analysis. It was found to be negligible at high x_L but to increase up to 8% at $x_L = 0.56$;
- migrations from low Q^2 were studied using the two MC samples described in section 4 and found to be $(11.2 \pm 0.5)\%$. Since no dependence on the proton variables x_L and p_T^2 was observed, a constant fraction was subtracted in each bin of the analysis;
- the overlay events which survived the $E + p_Z > 1655$ GeV cut described in section 3, were estimated using the x_L, p_T^2 spectrum of the tracks reconstructed in the LPS in randomly triggered events; these tracks were mixed with DIS events which did not have a proton in the LPS. This background was typically a few %, reaching $(7 \pm 3)\%$ in the bin $x_L > 0.98$.

7 Systematic uncertainties

To study the dependence of the results on the simulation of the physical processes, the detector and the beamline elements and on the analysis cuts, the measurement was repeated varying one at a time the following conditions:

- the $|V_Z|$ cut was varied by ± 10 cm;
- the cut on the scattered-electron energy was varied by ± 2 GeV and the CAL region in the transverse plane close to the beampipe which was excluded was increased by 0.5 cm in the X and Y directions;
- the $E - p_Z$ cut was changed to $35 < E - p_Z < 68$ GeV and to $41 < E - p_Z < 62$ GeV;
- the Δ_{pipe} threshold was varied by ± 0.02 cm, while the Δ_{pot} by 0.01 cm;
- the slope of the generated p_T^2 distribution in the MC was reweighted to 6.6 and 7.4 GeV^{-2};
- the fraction of overlay events to be subtracted from the data was increased and decreased by its statistical uncertainty; the fraction of π^+ and K^+ was varied by $\pm 21\%$ as suggested by the maximum value of the statistical uncertainty for this fraction obtained by the MC and by a study of the double coincidences of tracks in the LPS and neutrons in the ZEUS forward-neutron calorimeter [16];
- the bins in the x_L, p_T^2 plane were rejected according to a different criterion.

The effect of each systematic check was typically within the statistical uncertainty of the measurement, except for a few bins where the restriction of the $E - p_Z$ range, the increase of the scattered-positron energy cut and the selection of the x_L, p_T^2 bins produced an effect between one and two times the statistical uncertainty.

8 Results

The cross section $d\sigma_{ep\to eXp}/dx_L$ measured in the kinematic range $x_L > 0.56$, $p_T^2 < 0.5$ GeV^2, $Q^2 > 3\,\text{GeV}^2$ and $45 < W < 225$ GeV is shown in Fig. 3. It is found to be flat up to the diffractive peak, where it becomes approximately five times larger. Below the diffractive peak, the measurement contains the double-dissociative diffractive reaction, in which the beam proton dissociates.

The cross section $d\sigma_{ep\to eXp}/dp_T^2$, shown in Fig. 4, is found to decrease by an order of magnitude when p_T^2 goes from zero to 0.5 GeV^2. A fit to a single-exponential function in the full x_L range of the measurement returns a large χ^2/NDF; this is explained by the fact that the exponential fall of the cross section for $p_T^2 < 0.2$ GeV^2 is observed to be more

rapid than for $p_T^2 > 0.2$ GeV^2. Therefore, in Fig. 4 we limit ourselves to superimposing the curve $e^{-6.7 \cdot p_T^2}$ on our data for illustration.

Figure 5 shows the double-differential cross section $d^2\sigma_{ep \to eXp}/dx_L dp_T^2$ as a function of p_T^2 in bins of x_L. The p_T^2 range in each of the x_L bin of the measurement is dictated by the acceptance of the LPS-stations S4, S5 and S6, used for this study. In the Figure, the result of a single-exponential fit to the function $e^{-b \cdot p_T^2}$ in each of the x_L bins is superimposed to the data. The values of the b slope obtained from the fits are reported in Fig. 6, together with those measured by ZEUS using the 1995 LPS data [7]. The two measurements are consistent. The higher precision of this study reveals that the lower b-slope values measured around $x_L = 0.7$ and 0.9 should be ascribed to the smaller p_T^2 range of the measurement in these regions, imposed by the LPS acceptance, together with the fact that the slope for $p_T^2 < 0.2$ GeV^2 is steeper than for $p_T^2 > 0.2$ GeV^2. Therefore, we conclude that there is no evidence for an x_L dependence of the p_T^2 slope in our data.

9 Summary

The cross sections for the production of a leading proton in deep-inelastic scattering at $Q^2 > 3$ GeV^2 have been measured in the kinematic range $Q^2 > 3\,\text{GeV}^2$ and $45 < W < 225$ GeV. The data sample of 12.8 pb^{-1} collected with the ZEUS leading-proton spectrometer during 1996-97, allows a high-precision measurement in the kinematic region of the scattered proton $x_L > 0.56$ and $p_T^2 < 0.5$ GeV^2. Our data confirm the weak dependence of leading baryon production as a function of x_L measured in hadron-hadron collisions below the diffractive peak. The cross sections as a function of p_T^2 show an approximate exponential fall, which can be quantified by a slope $b \approx 6.7$ GeV^2. No visible dependence of b vs. x_L is observed.

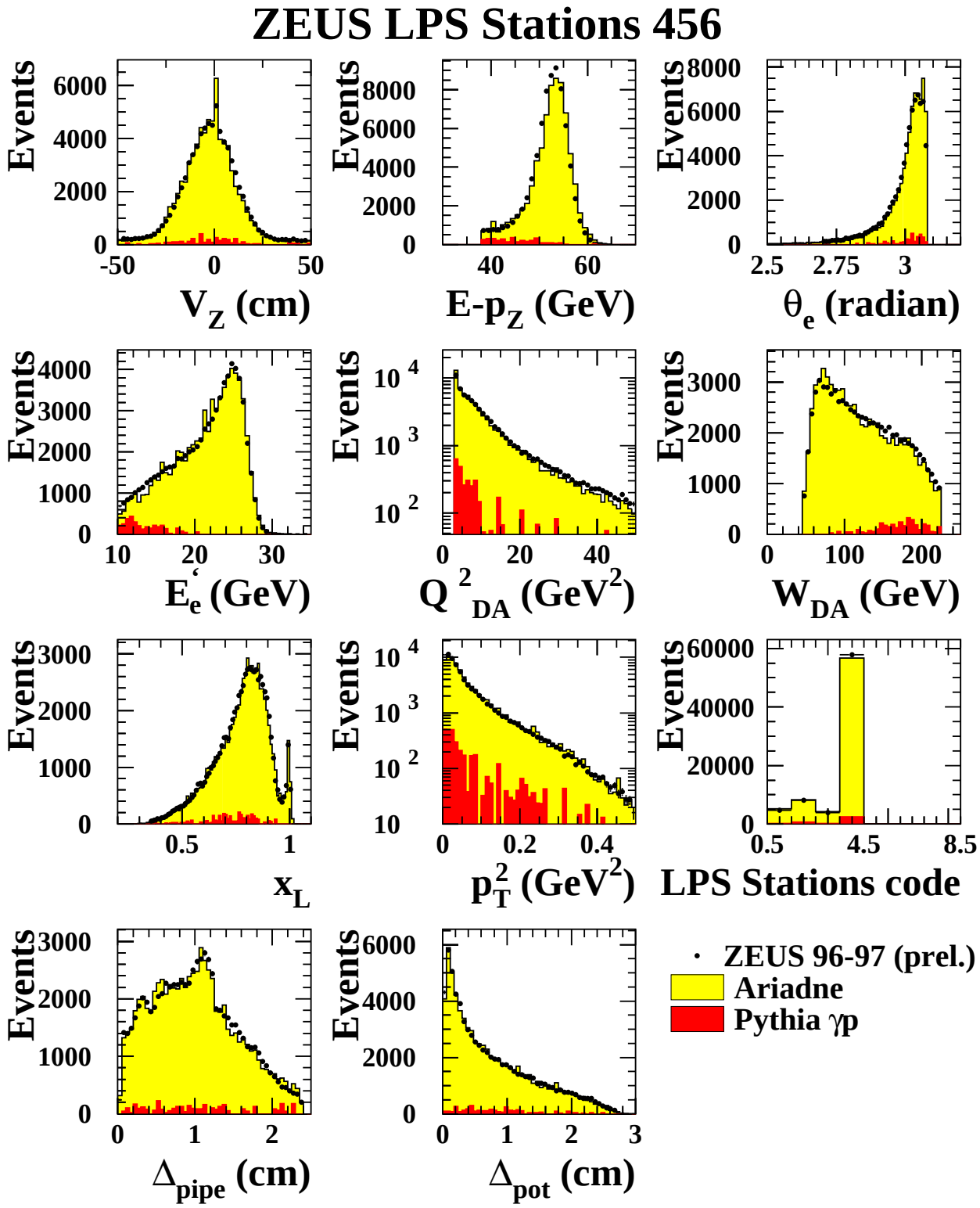

Figure 1: *Comparison between data and reweighted MC for several quantities described in the text. The dots represent the data; the light-shadowed histograms show the weighted sum of the two Djangoh MC samples described in the text, while the dark-shadowed histograms the Pythia photoproduction sample.*

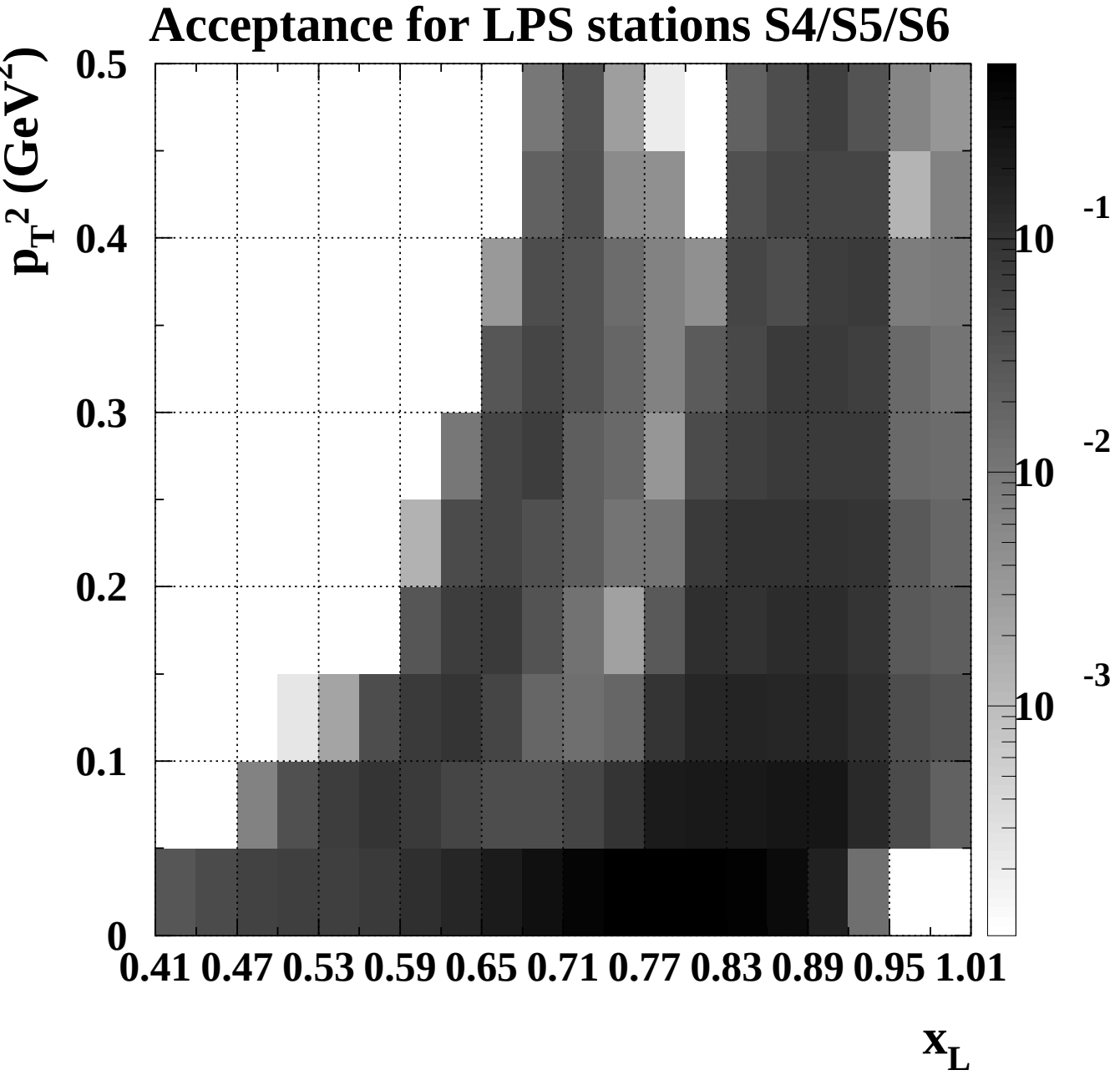

Figure 2: *Acceptance of the LPS stations S4, S5 and S6 in the x_L, p_T^2 plane.*

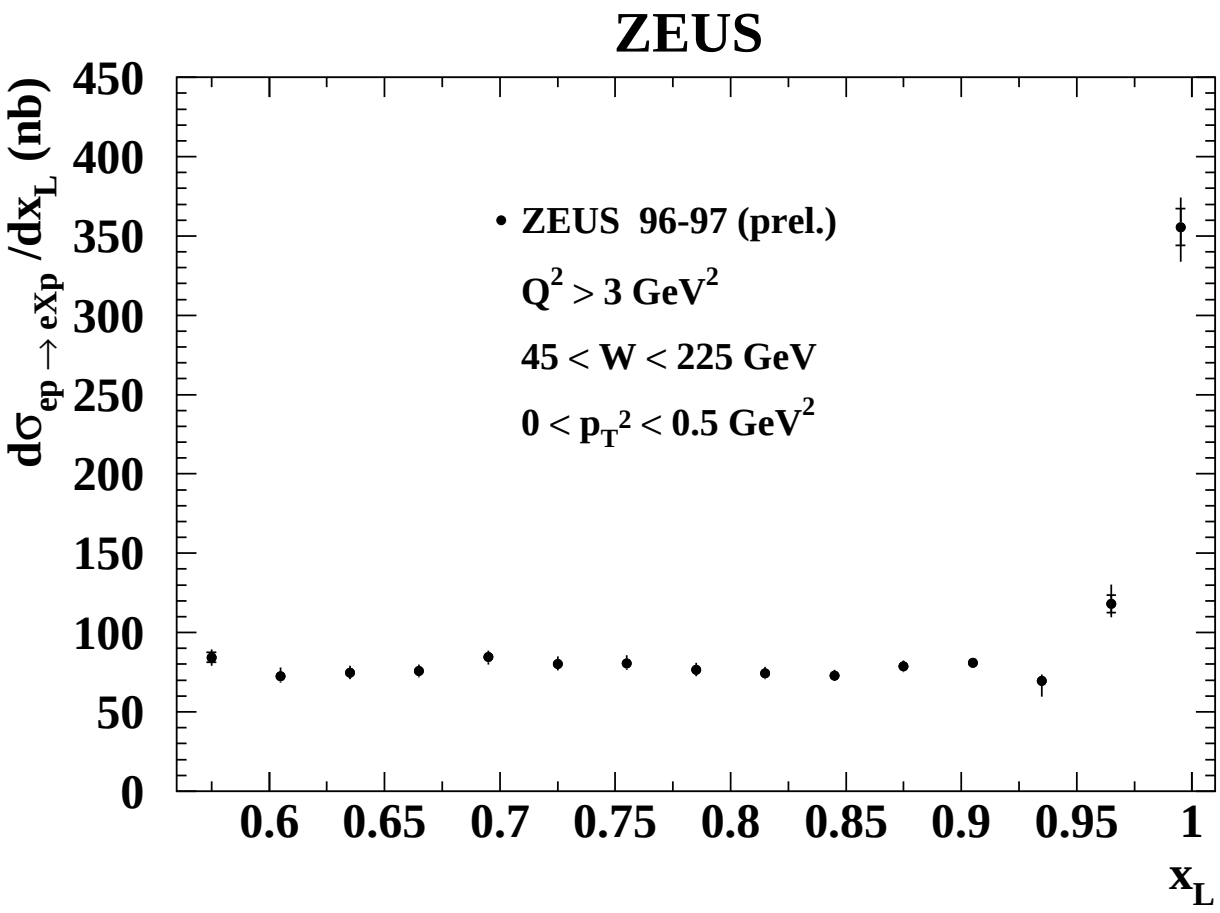

Figure 3: *The single differential cross section $d\sigma_{ep\to eXp}/dx_L$ measured in the kinematic range $x_L > 0.56$, $p_T^2 < 0.5$ GeV^2, $Q^2 > 3\,\mathrm{GeV}^2$ and $45 < W < 225$ GeV. The inner vertical bar on each measurement shows the statistical uncertainty, while the outer one the statistical and systematic uncertainties added in quadrature.*

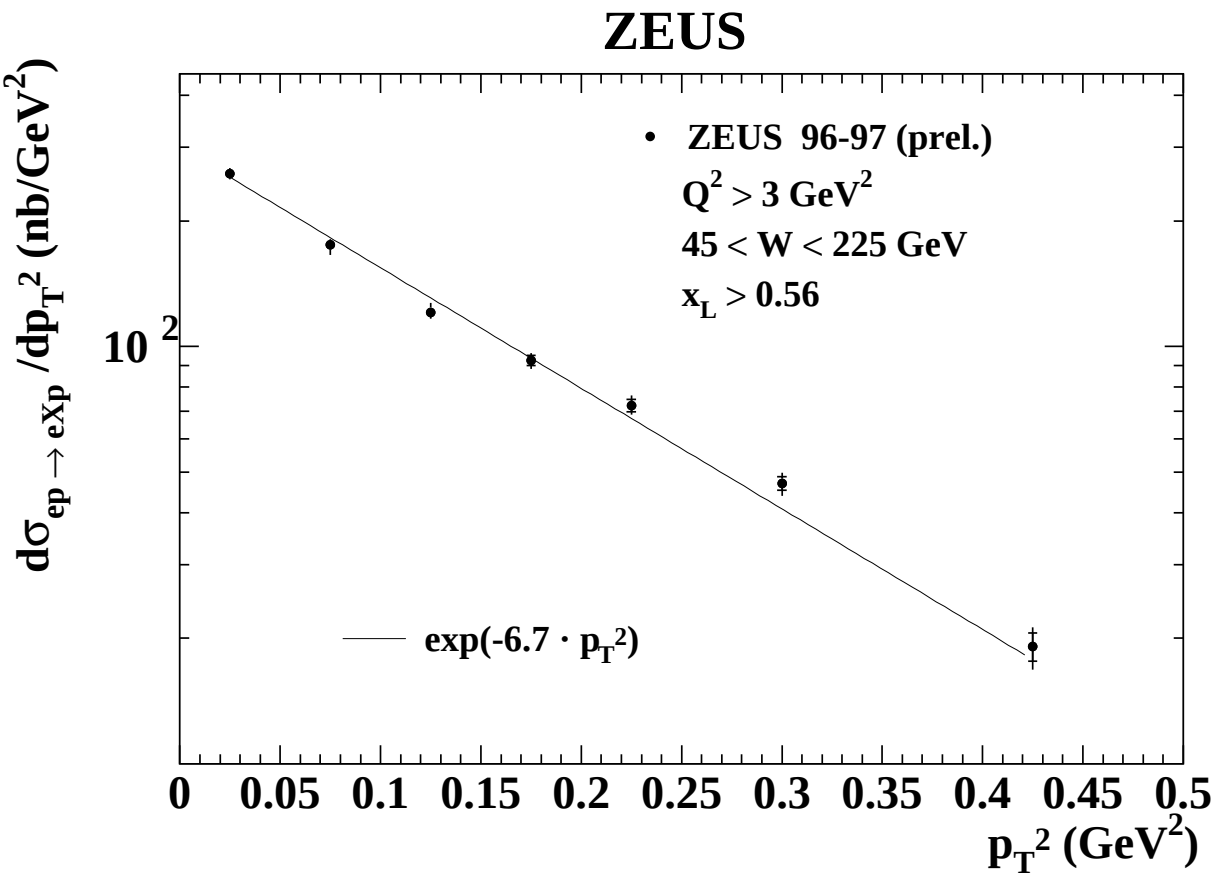

Figure 4: *The single differential cross section $d\sigma_{ep\to eXp}/dp_T^2$ measured in the kinematic range $x_L > 0.56$, $p_T^2 < 0.5$ GeV^2, $Q^2 > 3\,\mathrm{GeV}^2$ and $45 < W < 225$ GeV. The line shows the function $e^{-6.7\cdot p_T^2}$ normalised to the data. The inner vertical bar on each measurement shows the statistical uncertainty, while the outer one the statistical and systematic uncertainties added in quadrature.*

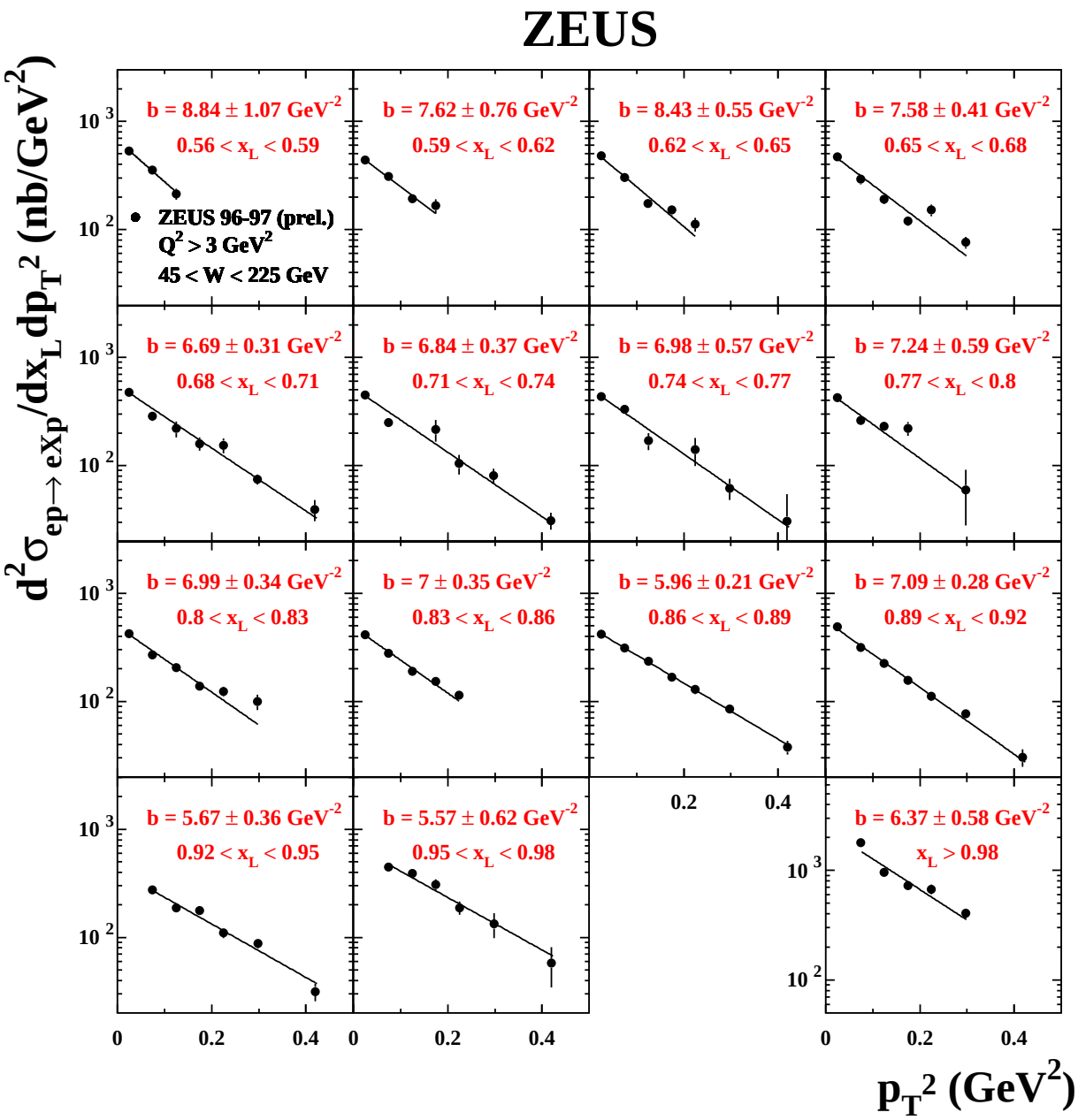

Figure 5: *The double-differential cross section $d^2\sigma_{ep\to eXp}/dx_L dp_T^2$ plotted as a function of p_T^2 in bins of x_L. The lines are the result of a fit to the function $A \cdot e^{-b \cdot p_T^2}$.*

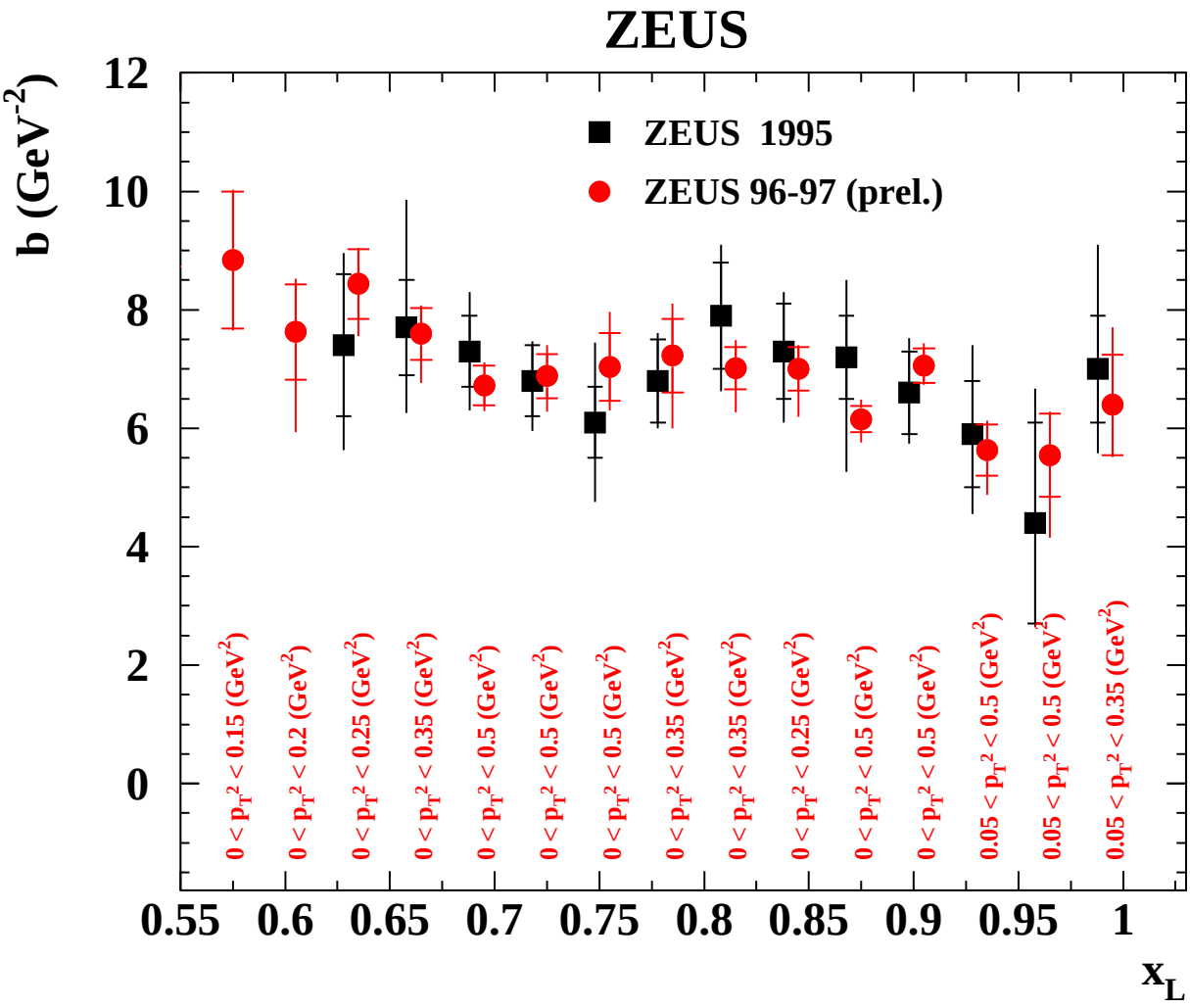

Figure 6: *The slope of the cross section $d\sigma_{ep\to eXp}/dp_T^2$ as obtained by the fit to the function $A{\cdot}e^{-b{\cdot}p_T^2}$ in bins of x_L . The full circles represent the present measurement, while the squares are the published ZEUS data [ref]. The inner vertical bar on each measurement shows the statistical uncertainty, while the outer one the statistical and systematic uncertainties added in quadrature. The range in p_T^2 used in each x_L bin of the present study is reported at the bottom of the measurement.*

References

[1] M. Basile et al., Lett. Nuovo Cimento **32**, 321 (1981).

[2] V.N. Gribov et al., L.N. Lipatov (ed.), World Scientific Series in 20th Century Physics **25** (2001).

[3] M. Aguilar-Benitez et al., Z. Phys. C **50**, 405 (1991).

[4] A. E. Brenner et al., Phys. Rev. D **26**, 1497 (1982).

[5] H1 Collab.,C. Adloff et al., Nucl. Phys. B **619**, 3 (2001).

[6] H1 Collab.,C. Adloff et al., Eur. Phys. J. C **6**, 587 (1999).

[7] ZEUS Collab.,S. Chekanov et al., Nucl. Phys. B **685**, 3 (2002).

[8] M. Basile et al., Nuovo Cimento **79A**, 1 (1984).

[9] ZEUS Collab.,M. Derrick et al., Z. Phys. C **3**, 253 (1997).

[10] ZEUS Coll., U. Holm (ed.), *The ZEUS Detector*. Status Report (unpublished), DESY (1993), available on `http://www-zeus.desy.de/bluebook/bluebook.html`.

[11] M. Derrick et al., Nucl. Inst. Meth. **A 309**, 77 (1991);
A. Andresen et al., Nucl. Inst. Meth. **A 309**, 101 (1991);
A. Caldwell et al., Nucl. Inst. Meth. **A 321**, 356 (1992);
A. Bernstein et al., Nucl. Inst. Meth. **A 336**, 23 (1993).

[12] N. Harnew et al., Nucl. Inst. Meth. **A 279**, 290 (1989);
B. Foster et al., Nucl. Phys. Proc. Suppl. **B 32**, 181 (1993);
B. Foster et al., Nucl. Inst. Meth. **A 338**, 254 (1994).

[13] F. Jacquet and A. Blondel, *Proceedings of the Study for an ep Facility for Europe*, U. Amaldi (ed.), p. 391. Hamburg, Germany (1979). Also in preprint DESY 79/48.

[14] H. Spiesberger, HERACLES *and* DJANGOH*: Event Generation for ep Interactions at HERA Including Radiative Processes*, 1998, available on `http://www.desy.de/~hspiesb/djangoh.html`.

[15] T. Sjöstrand et al., Comp. Phys. Comm. **135**, 238 (2001).

[16] ZEUS Coll., FNC group, S. Bhadra et al., Nucl. Inst. Meth. **A 394**, 121 (1997).